R. T. Steven, M. Niehaus, A. J. Taylor, A. Nasif, E. Elia, R. J. A. Goodwin, Zoltan Takats, J. Bunch

Atmospheric-Pressure Infrared Laser-Ablation Plasma-Postionization Mass Spectrometry Imaging of Formalin-Fixed Paraffin-Embedded (FFPE) and Fresh-Frozen Tissue Sections with No Sample Preparation

Rory T. Steven,* Marcel Niehaus, Adam J. Taylor, Ammar Nasif, Efstathios Elia, Richard J. A. Goodwin, Zoltan Takats, and Josephine Bunch*

ACCESS | Metrics & More | Article Recommendations | SI Supporting Information

ABSTRACT: Mass spectrometry imaging (MSI) encompasses a powerful suit of techniques which provide spatially resolved atomic and molecular information from almost any sample type. MSI is now widely used in preclinical research to provide insight into metabolic phenotypes of disease. Typically, fresh-frozen tissue preparations are considered optimal for biological MSI and other traditional preservation methods such as formalin fixation, alone or with paraffin embedding (FFPE), are considered less optimal or even incompatible. Due to the prevalence of FFPE tissue storage, particularly for rare and therefore high-value tissue samples, there is substantial motivation for optimizing MSI methods for analysis of FFPE tissue. Here, we present a novel modality, atmospheric-pressure infrared laser-ablation plasma postionization (AP-IR-LA-PPI), with the first proof-of-concept examples of MSI

Sample preparation free analysis of FFPE and fresh tissue by MSI

for FFPE and fresh-frozen tissues, with no post-sectioning sample preparation. We present ion images from FFPE and fresh tissues in positive and negative ion modes. Molecular annotations (via the Metaspace annotation engine) and on-tissue MS/MS provide additional confidence that the detected ions arise from a broad range of metabolite and lipid classes from both FFPE and fresh-frozen tissues.
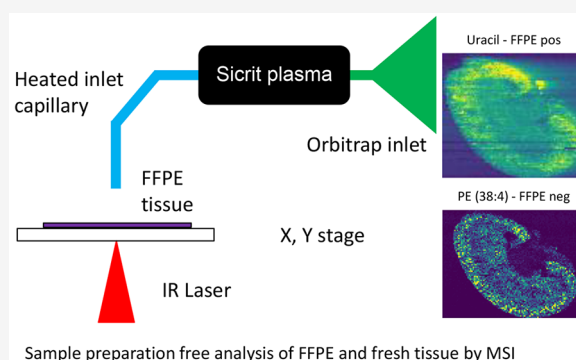
Archival storage of human tissues is routine practice, typically involving formal fixation and paraffin-embedding (FFPE) methods. Preservation by FFPE allows room temperature storage, enabling effective analysis of tissues many decades later.[1,2] Despite these positive characteristics, for mass spectrometry imaging (MSI) analysis, there are concerns relating to the washing out of soluble molecules during the fixation and dehydration steps of the FFPE process. The resulting presence of paraffin subsequently prevents the analysis of FFPE tissues by MSI without further, potentially deleterious, sample preparation steps. These heating, solvent wash, and antigen retrieval steps are also likely to delocalize and remove compounds of interest such as metabolites and lipids.[3]

MSI of FFPE tissues has been carried out for protein and peptide analyses,[4] and more recently, the reproducibility of these methods via interlaboratory studies have been evaluated.[5] Analysis of metabolites in FFPE tissues by MSI was shown for the first time by Walch and co-workers.[3] Antigen retrieval steps in these workflows can be omitted when targeting metabolite and lipid analyses. Despite this, a recent publication on the analysis of FFPE tissue by MSI for lipid detection has shown

that retaining the antigen retrieval step may, in fact, be beneficial for certain lipid classes.[6] Analysis of FFPE tissue was also recently carried out with a novel device (SpiderMass) and glycerol/IPA tissue treatment.[7] While these reports show great promise, improvements in both the range of species detected and the reduction or removal of additional sample processing would be beneficial.

Matrix-assisted laser desorption ionization (MALDI) MSI analysis of FFPE, fresh, or other tissue also requires addition of a matrix chemical. Introduction of this coating is known to potentially introduce artifacts such as analyte delocalization by crystal formation[8] or solvent[9,10] or exposure to vacuum in sublimation deposition.[11] Therefore, development of matrix-free methods is additionally desirable.

Postionization for MSI at atmospheric pressure has developed rapidly in recent years with dielectric barrier discharge (DBD) devices[12] being employed to interact with ejected plume material and ionize molecules present. Using a low temperature plasma (LTP) pen device, several groups have demonstrated the promise of plasma postionization. Moon and co-workers first introduced AP MSI with plasma postionization for small molecules.[13] Our own work demonstrated AP MALDI and LDI plasma postionization MSI for lipid analysis.[14,15] Winkler and co-workers employed matrix-free AP LDI plasma for analysis of plant tissue.[16] Recently, a commercially available in-line DBD plasma device became available, with its first demonstration for AP MALDI MSI plasma postionization[17] and subsequent AP LDI MSI in different configurations.[18,19] Infrared lasers have been used for AP (MA)LDI MSI with electrospray as the postionization method, termed LAESI or MALDESI.[20] These important studies have shown the promise of IR MALDESI for tissue imaging, primarily although not exclusively with water ice as the matrix.[21,22]

Within the study presented here, a novel ion source, atmospheric-pressure infrared laser-ablation plasma postionization (AP-IR-LA-PPI) MSI, is introduced (see Supporting Information (SI), SI Figure S1). With no post-tissue-sectioning sample preparation, proof-of-concept MSI data from fresh-frozen (FF) and formalin-fixed paraffin-embedded (FFPE) tissues were collected and analyzed. The data sets were uploaded to Metaspace[23] (see SI for web link to view data and materials and methods information), and these outputs are used to make preliminary assessments of metabolite and lipid detection from FFPE and fresh-frozen tissues. The relationship for inlet capillary temperature and example mean on-tissue negative ion spectra from FFPE kidney tissue are shown in Figure 1 with negative ion FF and positive ion spectra shown in SI Figures S2 and S3. Example plasma background spectra are shown in SI Figure S4, and example images for background ions are shown in SI Figure S5.

The inlet capillary temperature was found to influence detected ion intensity with varying optima observed for different species in FF and FFPE tissues. Two examples are shown for glutamine and PE (38:5) assigned ions from FFPE kidney tissue (Figure 1A and B) showing optimal temperatures of ~250 and 400 °C, respectively. The background ion signal increases at higher temperatures for glutamine, although this is not observed in the equivalent FF tissue data (SI Figure S6). Subsequent MSI experiments were carried out with capillary temperatures of 250 and 400 °C for low (80−305 Da) and high (300−1000 Da) mass range data sets, respectively (Figure 1C and D, SI Figures S2 and S3) to align with these approximate optimal temperatures. These trends indicate complex interaction involving analyte physicochemical properties, plume dynamics and inlet parameters. Therefore, mechanistic studies will be of great interest in the future.

Rich spectra were observed across all examined tissues with candidates from a variety of molecular classes readily observed. No clear tissue endogenous species were observed without plasma postionization. Prominent peaks are labeled with Metaspace annotations in Figure 1C and D and SI Figures S2 and S3, providing examples of the spectral information obtained from each of these samples and polarities, although multiple assigned identities are possible for many ions, as is typical. The number of assigned identities are similar to other data sets in Metaspace collected by more established methods
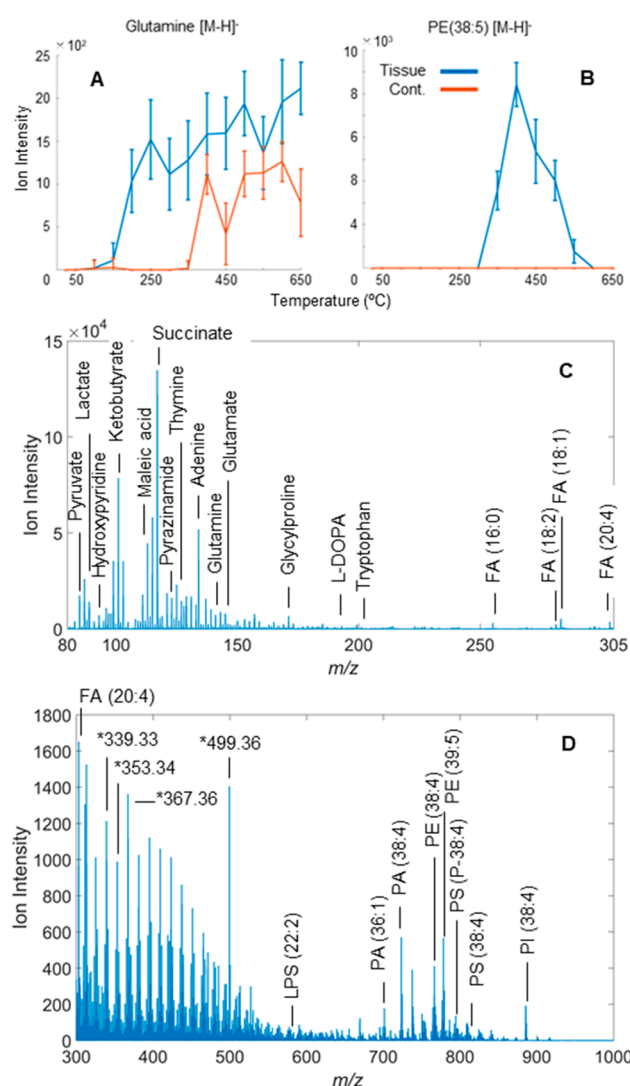

Figure 1. Ion intensity vs inlet capillary temperature for (A) glutamine and (B) PE (38:5) in FFPE tissue and mean negative ion mode on-tissue spectra from low (C) and high (D) *m/z* FFPE kidney tissue MSI data sets. Ions denoted with *m/z* and an asterisk are example background ions.

such as MALDI and DESI MSI and compare favorably to many (SI Table S1). The number and range of the assigned species show the promise of this tissue sampling and ionization configuration for sample preparation-free analysis of FFPE and FF tissues. The FFPE and FF kidney tissues are not matched tissues, shown from the mean spectra in Figure 1 and SI Figures S2 and S3), so quantitative comparisons should not be made between them. However, these data will still function well as a guide for detection of predominant ions in these tissues and as a general indication of the performance of this ion source. Example ion images from negative and positive FFPE and FF tissue data are shown in Figure 2. Qualitatively, all data sets collected show a large number and variety of ion images corresponding to kidney histology, comparable to similar pixel size MS images from fresh-frozen kidney analyzed by more common modalities such as MALDI or DESI.[24−26] These images show a range of distributions corresponding to aspects of kidney anatomy. The displayed negative ion FFPE data show some relatively homogeneous distributions in, for example, succinate (*m/z* 117.0192) and adenine (*m/z*
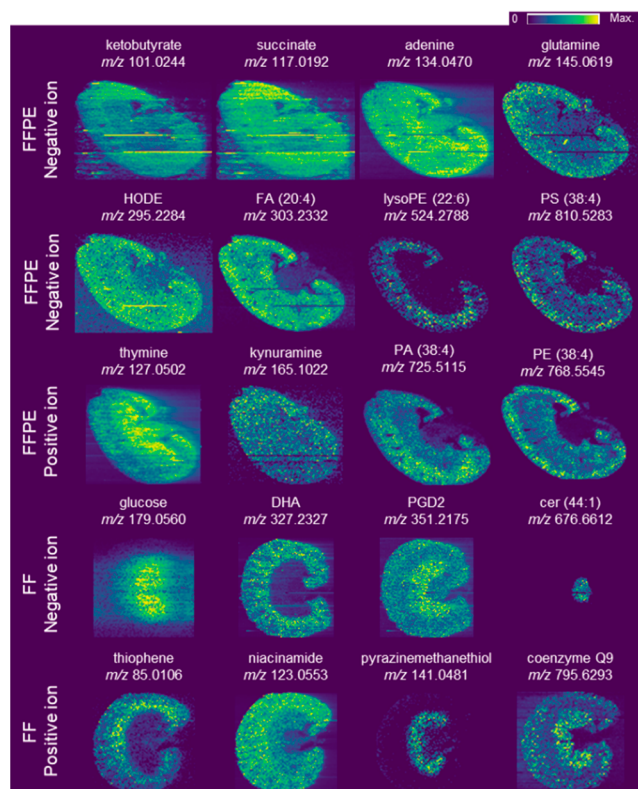
Figure 2. Example images from FFPE and FF, negative and positive ions identified by Metaspace. Numerous endogenous ions are detected with good signal intensities and a variety of spatial distributions for FFPE and FF tissues.

134.0470) as well as ions more prominently localized in the cortex (lysoPE (22:6)) (m/z 524.2788). Within the FF data, glucose (m/z 179.0560) shows highest intensity in the medulla, and the distribution of Cer (44:1) (m/z 676.6612) is localized exclusively within the approximate renal pelvis region, a little observed distribution within these data. Additionally, the assignment of kynuramine (Figure 2, FFPE positive ion, m/z 165.1022) and niacinamide indicate the potential strength of this ion source as an alternative to, for example, MALDI or DESI, as these molecules are assigned in very few data sets in Metaspace. On-tissue MS/MS data were also acquired for both FFPE and FF samples with 18 ions showing matched fragments, supporting their identities by MyCompoundID[27] including succinate, kynuramine, glucose, niacinamide, vitamin D, HODE, FA (20:4), and PS (38:4) (SI Table 2).

When reviewing these data sets in Metaspace, assignments are present which are more associated with the background signal rather than tissue endogenous ions, potentially indicating that their assignments are erroneous. These ions may derive from paraffin in the case of FFPE tissue, from plasma-ionized laboratory air, from capillary carry-over phenomena, and fragmentation products. We include additional discussion on the background signal for these data in the SI (page S11). Erroneous assignments of background ions are common when automating assignment in MSI generally and indicate that caution is still necessary when interpreting putative assignments.

Further to spectral summaries and example images, an evaluation of the common chemical annotations provided by

Metaspace is presented. Example images for the unique and shared annotations across the tissues and polarities are shown in Figure 3. Molecular assignments for FF and FFPE kidney
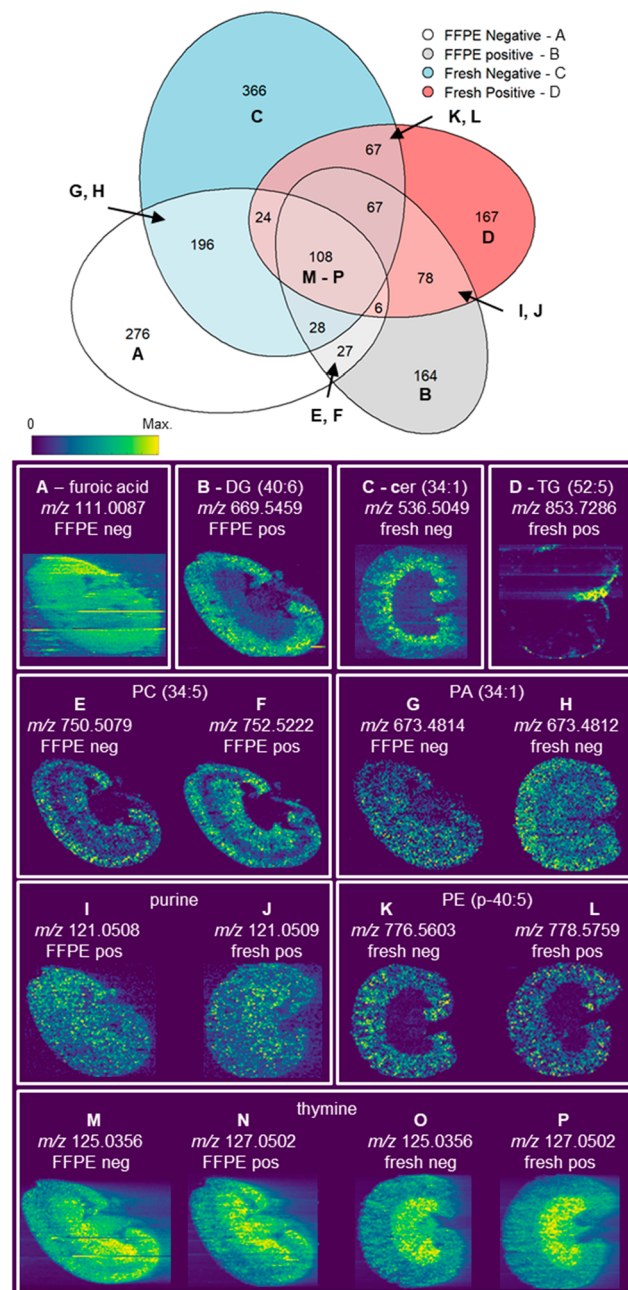

Figure 3. Summary of unique molecular identities with example ion images for positive and negative ion modes and FFPE and FF mouse kidney tissue MSI data. (Top) Euler plot showing set intersection for all Metaspace coannotated chemical formulas for each tissue and polarity. (A−P, bottom) Example ion images corresponding to the same letter- and color-labeled regions of the Euler plot, giving examples of uniquely or codetected ions across polarities or tissues.

tissues MSI data sets show both common and unique identities. The Euler plot (Figure 3, top) shows the set intersections for coannotated chemical formulas.

As expected from the spectral overviews (Figure 1, SI Figures S2 and S3), there is overlap of assignments between the FF and FFPE tissues for a given polarity, but additionally,

there is overlap between positive and negative ion mode data sets as well, although to a lesser extent. Example ion images are also shown in the lower portion of Figure 2, with all Metaspace-derived putative IDs shown corresponding to either $[M + H]^+$ or $[M - H]^-$ ions. Ion images A−P (Figure 3) are displayed as examples of the primary regions in the Euler plot, with letter-matched labels. Here, images of uniquely matched ions are shown across A−D. Images of assigned ions common to two data sets are shown from E to L and across all four data sets from M to P. As discussed, a portion of these ions may be incorrectly assigned, but we still consider this evaluation of coannotation to be informative. Encouragingly, given the very different sample processing steps applied to FFPE tissue compared to FF, those ions with shared matched identities also show similar spatial distributions, either between FFPE and FF (G/H, I/J), positive and negative ion (E/F, K/L), or across all four (M−P). Several interesting spatial distributions are also observed here including image D, where a distribution in the pelvic region (or local adipose tissue) and parts of the capsule are seen, in common with a similar recently published TG distribution in MALDI MSI.[28]

The study presented here goes beyond previous approaches for the analysis of FFPE tissue removing the need for all sample pretreatment when analyzing FFPE tissues. This approach enables the detection and imaging of a broad range of low mass metabolite and lipid species to complement more common approaches such as UV-MALDI and DESI MSI. Removing the need for additional sample preparation is potentially of great benefit for FFPE tissue due to the likely deleterious influence of wax removal on metabolites and lipids that have survived the initial FFPE process. Further, the need to add a matrix for MALDI analysis can be avoided, removing another sample preparation step that can bias ionization and cause analyte migration prior to analysis. The ability to analyze material without sample preparation may also prove powerful for native MSI of biological samples. This promising new ion source can allow FFPE and other "incompatible" sample forms to be analyzed more readily by MSI and, in the future, potentially bring great added value to the suite of MSI techniques available to the community.

■ ASSOCIATED CONTENT

ⓈⒾ Supporting Information

The Supporting Information is available free of charge at https://pubs.acs.org/doi/10.1021/acs.analchem.2c00690.

> Materials and methods, positive ion mode FFPE and FF and negative ion FF tissue spectral summaries, MS/MS summary table, and author contributions (PDF)

■ AUTHOR INFORMATION

Corresponding Authors

Rory T. Steven − National Centre of Excellence in Mass Spectrometry Imaging, National Physical Laboratory, Teddington TW12 0WL, United Kingdom; ⓞ orcid.org/0000-0002-6754-2424; Email: rory.steven@npl.co.uk

Josephine Bunch − National Centre of Excellence in Mass Spectrometry Imaging, National Physical Laboratory, Teddington TW12 0WL, United Kingdom; Faculty of Medicine, Department of Metabolism, Digestion and Reproduction, Imperial College London, London SW7 2AZ, United Kingdom; Biological Mass Spectrometry, Rosalind Franklin Institute, Didcot OX11 0QS, United Kingdom; Email: josephine.bunch@npl.co.uk

Authors

Marcel Niehaus − National Centre of Excellence in Mass Spectrometry Imaging, National Physical Laboratory, Teddington TW12 0WL, United Kingdom; Present Address: Marcel Niehaus: Bruker Daltonics GmbH & Co.KG, Fahrenheitstrasse 4, 28359 Bremen, Germany; ⓞ orcid.org/0000-0002-4876-6190

Adam J. Taylor − National Centre of Excellence in Mass Spectrometry Imaging, National Physical Laboratory, Teddington TW12 0WL, United Kingdom; Present Address: Adam Taylor: Sage Bionetworks, 2901 3rd. Ave, Suite 330, Seattle, Washington 98121, USA.; ⓞ orcid.org/0000-0003-0501-8886

Ammar Nasif − National Centre of Excellence in Mass Spectrometry Imaging, National Physical Laboratory, Teddington TW12 0WL, United Kingdom

Efstathios Elia − National Centre of Excellence in Mass Spectrometry Imaging, National Physical Laboratory, Teddington TW12 0WL, United Kingdom; ⓞ orcid.org/0000-0003-2769-7066

Richard J. A. Goodwin − Imaging and Data Analytics, Clinical Pharmacology and Safety Sciences, BioPharmaceuticals R&D, AstraZeneca, Cambridge CB2 0WG, United Kingdom; Institute of Infection, Immunity and Inflammation, College of Medical, Veterinary and Life Sciences, University of Glasgow, Glasgow G12 8TA, United Kingdom

Zoltan Takats − Faculty of Medicine, Department of Metabolism, Digestion and Reproduction, Imperial College London, London SW7 2AZ, United Kingdom; Biological Mass Spectrometry, Rosalind Franklin Institute, Didcot OX11 0QS, United Kingdom; ⓞ orcid.org/0000-0002-0795-3467

Complete contact information is available at:
https://pubs.acs.org/10.1021/acs.analchem.2c00690

Notes

The authors declare no competing financial interest.

■ ACKNOWLEDGMENTS

■ REFERENCES

(1) Paine, M. R. L.; Ellis, S. R.; Maloney, D.; Heeren, R. M. A.; Verhaert, P. D. E. M. Anal. Chem. 2018, 90, 9272−9280.

(2) Grillo, F.; Bruzzone, M.; Pigozzi, S.; Prosapio, S.; Migliora, P.; Fiocca, R.; Mastracci, L. Journal of Clinical Pathology 2017, 70, 988−993.

(3) Buck, A.; Ly, A.; Balluff, B.; Sun, N.; Gorzolka, K.; Feuchtinger, A.; Janssen, K.-P.; Kuppen, P. J.; van de Velde, C. J.; Weirich, G.; Erlmeier, F.; Langer, R.; Aubele, M.; Zitzelsberger, H.; Aichler, M.; Walch, A. Journal of Pathology 2015, 237, 123−132.

(4) Aoki, Y.; Toyama, A.; Shimada, T.; Sugita, T.; Aoki, C.; Umino, Y.; Suzuki, A.; Aoki, D.; Daigo, Y.; Nakamura, Y.; Sato, T.-A. Proceedings of the Japan Academy, Series B 2007, 83, 205−214.

(5) Buck, A.; Heijs, B.; Beine, B.; Schepers, J.; Cassese, A.; Heeren, R. M.; McDonnell, L. A.; Henkel, C.; Walch, A.; Balluff, B. *Anal Bioanal Chem.* **2018**, *410*, 5969−5980.

(6) Denti, V.; Piga, I.; Guarnerio, S.; Clerici, F.; Ivanova, M.; Chinello, C.; Paglia, G.; Magni, F.; Smith, A. *J. Am. Soc. Mass Spectrom.* **2020**, *31*, 1619−1624.

(7) Ogrinc, N.; Attencourt, C.; Colin, E.; Boudahi, A.; Tebbakha, R.; Salzet, M.; Testelin, S.; Dakpe, S.; Fournier, I. *Frontiers in Oral Health* **2022**, *3*, 827360.

(8) Passarelli, M. K.; Wang, J.; Mohammadi, A. S.; Trouillon, R.; Gilmore, I.; Ewing, A. G. *Anal. Chem.* **2014**, *86*, 9473−9480.

(9) Steven, R. T.; Race, A. M.; Bunch, J. *J. Am. Soc. Mass Spectrom.* **2013**, *24*, 801−804.

(10) Anderson, D. M. G.; Floyd, K. A.; Barnes, S.; Clark, J. M.; Clark, J. I.; McHaourab, H.; Schey, K. L. *Anal Bioanal Chem.* **2015**, *407*, 2311−2320.

(11) Van Nuffel, S.; Elie, N.; Yang, E.; Nouet, J.; Touboul, D.; Chaurand, P.; Brunelle, A. *Anal. Chem.* **2018**, *90*, 1907−1914.

(12) Nudnova, M. M.; Sigg, J. r. m.; Wallimann, P.; Zenobi, R. *Anal. Chem.* **2015**, *87*, 1323−1329.

(13) Kim, J. Y.; Seo, E. S.; Kim, H.; Park, J.-W.; Lim, D.-K.; Moon, D. W. *Nat. Commun.* **2017**, *8*, 2113.

(14) Steven, R. T.; Shaw, M.; Dexter, A.; Murta, T.; Green, F. M.; Robinson, K. N.; Gilmore, I. S.; Takats, Z.; Bunch, J. *Anal. Chim. Acta* **2019**, *1051*, 110−119.

(15) Yan, B.; Murta, T.; Elia, E. A.; Steven, R. T.; Bunch, J. *J. Am. Soc. Mass Spectrom.* **2021**, *32*, 429−435.

(16) Moreno-Pedraza, A.; Rosas-Román, I.; Garcia-Rojas, N. S.; Guillén-Alonso, H.; Ovando-Vázquez, C.; Díaz-Ramírez, D.; Cuevas-Contreras, J.; Vergara, F.; Marsch-Martínez, N.; Molina-Torres, J.; Winkler, R. *Anal. Chem.* **2019**, *91*, 2734−2743.

(17) Elia, E. A.; Niehaus, M.; Steven, R. T.; Wolf, J.-C.; Bunch, J. *Anal. Chem.* **2020**, *92*, 15285−15290.

(18) Lu, Q.; Xu, Z.; You, X.; Ma, S.; Zenobi, R. *Anal. Chem.* **2021**, *93*, 6232−6238.

(19) Funke, S. K. I.; Brückel, V. A.; Weber, M.; Lützen, E.; Wolf, J.-C.; Haisch, C.; Karst, U. *Anal. Chim. Acta* **2021**, *1177*, 338770.

(20) Robichaud, G.; Barry, J. A.; Muddiman, D. C. *J. Am. Soc. Mass Spectrom.* **2014**, *25*, 319−328.

(21) Bagley, M. C.; Ekelöf, M.; Rock, K.; Patisaul, H.; Muddiman, D. C. *Anal Bioanal Chem.* **2018**, *410*, 7979−7986.

(22) Hieta, J.-P.; Kopra, J.; Raikkonen, H.; Kauppila, T. J.; Kostiainen, R. *Anal. Chem.* **2020**, *92*, 13734−13741.

(23) Palmer, A.; Phapale, P.; Chernyavsky, I.; Lavigne, R.; Fay, D.; Tarasov, A.; Kovalev, V.; Fuchser, J.; Nikolenko, S.; Pineau, C.; Becker, M.; Alexandrov, T. *Nat. Methods* **2017**, *14*, 57−60.

(24) Swales, J. G.; Tucker, J. W.; Strittmatter, N.; Nilsson, A.; Cobice, D.; Clench, M. R.; Mackay, C. L.; Andren, P. E.; Takats, Z.; Webborn, P. J. H.; Goodwin, R. J. A. *Anal. Chem.* **2014**, *86*, 8473−8480.

(25) Shroff, E. H.; Eberlin, L. S.; Dang, V. M.; Gouw, A. M.; Gabay, M.; Adam, S. J.; Bellovin, D. I.; Tran, P. T.; Philbrick, W. M.; Garcia-Ocana, A.; Casey, S. C.; Li, Y.; Dang, C. V.; Zare, R. N.; Felsher, D. W. *Proc. Natl. Acad. Sci. U. S. A.* **2015**, *112*, 6539−6544.

(26) Smith, K. W.; Flinders, B.; Thompson, P. D.; Cruickshank, F. L.; Mackay, C. L.; Heeren, R. M. A.; Cobice, D. F. *ACS Omega* **2020**, *5*, 13430−13437.

(27) Huan, T.; Tang, C.; Li, R.; Shi, Y.; Lin, G.; Li, L. *Anal. Chem.* **2015**, *87*, 10619−10626.

(28) Fincher, J. A.; Djambazova, K. V.; Klein, D. R.; Dufresne, M.; Migas, L. G.; Van de Plas, R.; Caprioli, R. M.; Spraggins, J. M. *J. Am. Soc. Mass Spectrom.* **2021**, *32*, 2519−2527.